

Effect of supersonic relative motion between baryons and dark matter on collapsed objects

Shinsuke Asaba,^{1,*} Kiyotomo Ichiki,^{1,2} and Hiroyuki Tashiro¹

¹*Department of Physics, Graduate School of Science, Nagoya University, Aichi 464-8602, Japan*

²*Kobayashi-Maskawa Institute for the Origin of Particles and the Universe, Nagoya University, Aichi 464-8602, Japan*

(Received 2 September 2015; published 25 January 2016)

Great attention is given to the first star formation and the epoch of reionization as main targets of planned large radio interferometries (e.g. Square Kilometre Array). Recently, it is claimed that the supersonic relative velocity between baryons and cold dark matter can suppress the abundance of first stars and impact the cosmological reionization process. Therefore, in order to compare observed results with theoretical predictions it is important to examine the effect of the supersonic relative motion on the small-scale structure formation. In this paper, we investigate this effect on the nonlinear structure formation in the context of the spherical collapse model in order to understand the fundamental physics in a simple configuration. We show the evolution of the dark matter sphere with the relative velocity by both using N-body simulations and numerically calculating the equation of motion for the dark matter mass shell. The effects of the relative motion in the spherical collapse model appear as the delay of the collapse time of dark matter halos and the decrease of the baryon mass fraction within the dark matter sphere. Based on these results, we provide the fitting formula of the critical density contrast for collapses with the relative motion effect and calculate the mass function of dark matter halos in the Press-Schechter formalism. As a result, the relative velocity decreases the abundance of dark matter halos whose mass is smaller than $10^8 M_\odot/h$.

DOI: [10.1103/PhysRevD.93.023518](https://doi.org/10.1103/PhysRevD.93.023518)

I. INTRODUCTION

The standard cosmological model, called the Λ CDM model, composed with two relativistic species (photons and neutrinos), two nonrelativistic matters (baryons and dark matter), and the energy having negative pressure (dark energy) with a nearly scale-invariant spectrum of curvature perturbations, has achieved great success in explaining large-scale cosmological observations, e.g., large-scale structure formation [1] and cosmic microwave background [2].

The theoretical description of small-scale structure formation is, however, still debatable. Understanding of small-scale structure formation at high redshifts is essential to study first stars and the epoch of reionization (EoR). One expects redshifted 21 cm lines from the hyperfine structure of hydrogen atoms as the powerful probe for the EoR and first stars [3,4] and the matter density underlying HI distribution constrains extended parameters of the Λ CDM model [5–7]. Currently, to probe such small-scale structure formation, there are many planned observations including Murchison Widefield Array [8] and Square Kilometre Array (SKA) [9]. Therefore, nowadays, the detailed studies on small-scale structure formation at high redshifts attract a lot of attention.

Recently, Ref. [10] reports the importance of the supersonic relative motion between dark matter and baryons on small-scale structure formation related to the EoR. This

supersonic relative motion is originated from the difference in the motions between baryons and dark matter before recombination. Baryons before recombination are tightly coupled with photons by Thomson scattering. As a result, baryons and photons act as one fluid with the sound speed $\sim c/\sqrt{3}$ and have the velocity field associated with the acoustic oscillation. On the other hand, dark matter does not suffer from Thomson scattering and dark matter density fluctuations can grow gravitationally. Therefore, the relative motion between baryons and dark matter is induced. After recombination, baryons are fully decoupled with photons and the sound speed of baryons quickly drops to ~ 6 km/s. Since the root mean square of the relative velocity reaches ~ 30 km/s at that time, the relative velocity is about five times larger than the sound speed of baryons. Because the relative motion is highly supersonic, the effect on the structure formation could be significant. In particular, the abundance of small dark matter halos ($M \lesssim 10^7 M_\odot$) is highly suppressed due to the supersonic relative motion. This effect has been intensively studied by many authors with N-body/smoothed particle hydrodynamics (SPH) simulations [11–13]. Therefore, according to the effect on the structure formation, the scenario of the cosmic reionization and the prediction of the 21 cm line signals from the EoR could be modified from those predicted in the conventional cosmological model. The recent relevant studies are reviewed in Ref. [14].

So far the effects of the relative motion on the structure formation have been studied in numerical simulations

*asaba.shinsuke@j.mbox.nagoya-u.ac.jp

mainly, because these effects are complicated. However, a study with the analytical model is useful to obtain some insights into physics involved in complicated phenomena. Additionally the analysis of observation data with numerical simulations generally takes enormous time and, sometimes, it seems unrealistic. Therefore, modeling in a form which is easy to handle in analytic studies is highly required.

In the study on the structure formation, the halo mass function is one of the interesting quantities. In particular, the Press-Schechter formalism with the sphere collapse model provides the mass function in the analytical form which relatively agrees well with the results of N-body simulations.

In this paper, we revisit the effect of the supersonic relative motion on small-scale structure formation in the context of the spherical collapse model by both N-body simulations and a semianalytical way. The effect of the relative motion on the spherical collapse can be represented as the modification of the critical density contrast. We propose a fitting formula of the critical density contrast, as a function of the amplitude of the relative motion, the halo mass and the initial density fluctuation within dark matter halos. We also apply this fitting formula to evaluate the mass function of small dark matter halos based on the Press-Schechter formalism.

This paper is organized as follows. In Sec. II we review the effect of supersonic relative motion on the perturbation theory by taking into account the background velocity of baryons and construct the spherical collapse model with two components. In Sec. III we describe the setup of our N-body simulation, and we show the results of the N-body simulations and check the reproducibility of the spherical collapse in Sec. IV. Moreover we present the change of the collapse time by supersonic relative motion and the validity of the semi-analytical model introduced in Sec. II. Section V is devoted to the discussion of the relative motion effect on dark matter halos. We discuss the modification of the baryon fraction in a dark matter halo by the relative motion, and, providing a fitting formula of the modified collapse time (i.e. the critical density contrast for the collapse). We show the suppression of the dark matter halo abundance around the EoR as an application of our results. Finally we summarize this paper in Sec. VI.

II. ANALYTICAL FORMALISM

In this section, we show the effect of the supersonic relative motion between baryons and dark matter on the linear perturbation theory, and evaluate this effect on the nonlinear growth by adopting the spherical collapse model.

A. Perturbation theory

Since the supersonic relative motion between baryons and dark matter has been analytically studied in the

moving-background perturbation theory (MBPT) [10], we first make a brief review of the MBPT. The MBPT introduces the background peculiar velocity which corresponds to the relative velocity between baryons and dark matter, i.e. $\vec{v}^{\text{bg}} = \vec{v}_{bc}$. According to the energy momentum conservation equation with homogeneous background densities of baryons and dark matter, the evolution of \vec{v}_{bc} is in reverse proportion to the scale factor due to the cosmic expansion.

In the MBPT, the first order energy momentum conservation equations after recombination are given by

$$\begin{aligned} \frac{d\delta_c}{dt} &= -\theta_c, \\ \frac{d\theta_c}{dt} &= -\frac{3H^2}{2}(\Omega_c\delta_c + \Omega_b\delta_b) - 2H\theta_c, \\ \frac{d\delta_b}{dt} &= -\frac{i}{a}\vec{v}_{bc}\cdot\vec{k}\delta_b - \theta_b, \\ \frac{d\theta_b}{dt} &= -\frac{i}{a}\vec{v}_{bc}\cdot\vec{k}\theta_b - \frac{3H^2}{2}(\Omega_c\delta_c + \Omega_b\delta_b) - 2H\theta_b + \frac{c_s^2k^2}{a^2}\delta_b, \end{aligned} \quad (1)$$

where c_s is the sound velocity of the baryon fluid, the subscripts c and b denote cold dark matter and baryons respectively and $\theta = ia^{-1}\nabla\cdot\vec{v}$ represents the divergence of the peculiar velocity. In Eq. (1) we take the frame where the background velocity of cold dark matter is absent. In other words, $\vec{v}_b^{\text{bg}} = \vec{v}_{bc}$ and $\vec{v}_c^{\text{bg}} = 0$. For simplicity, we ignore perturbations of the sound velocity although they might affect the growth of the density fluctuation on small scales [15–17]. Equation (1) can be rewritten to the second order differential equations of the density fluctuations as

$$\begin{aligned} \frac{d^2\delta_c}{dt^2} &= -2H\frac{d\delta_c}{dt} + \frac{3H^2}{2}(\Omega_c\delta_c + \Omega_b\delta_b), \\ \frac{d^2\delta_b}{dt^2} &= -\left(2H + 2i\mu v_{bc}\frac{k}{a}\right)\frac{d\delta_b}{dt} + \frac{3H^2}{2}(\Omega_c\delta_c + \Omega_b\delta_b) \\ &\quad - (c_s^2 + \mu^2 v_{bc}^2)\frac{k^2}{a^2}\delta_b, \end{aligned} \quad (2)$$

where $\mu = \vec{v}_{bc}\cdot\vec{k}/|\vec{v}_{bc}||\vec{k}|$.

Equation (2) tells us that the relative motion prevents the growth of density fluctuations on small scales in the same way of the fluid pressure in the discussion of the Jeans instability. On large scales where the relative motion does not have the preferred direction, while the odd term of μ in the last equation of Eq. (2) vanishes by averaging over all random directions of the relative motion, the third term of the right-hand side is enhanced due to the existence of the term with v_{bc}^2 . As a result, the effective Jeans scale (the suppression scale) of Eq. (2) becomes large due to the existence of the relative velocity. Since the relative velocity after recombination is roughly $\langle v_{bc}^2 \rangle^{1/2} \sim 5c_s$,

the suppression scale for the relative motion is $k_{bc} = aH/\langle v_{bc}^2 \rangle^{1/2} \sim 40 \text{ hMpc}^{-1}$. The corresponding mass scale for the suppression is $M_{bc} \sim 10^7 M_\odot/h$.

However, when we consider a local sufficiently small patch, the odd term of μ cannot vanish in the patch. Instead, the relative motion in this patch can be assumed to be a homogeneous flow with one direction. In this case, when the relative velocity is larger than the Hubble flow, $\mu v_{bc} > k/aH$, the density fluctuations inside the patch start to grow exponentially due to the relative motion flow as shown in Eq. (2). The perturbation theory is not valid in this case, and we need to consider the effect of the relative velocity on the nonlinear growth, e.g., in the spherical collapse model.

B. Spherical collapse model

The spherical collapse model is a simple analytical model to investigate the nonlinear evolution of an overdensity region. In this model, the evolution of the overdensity region is described as the motion of the constant density spheres. Let us consider the collapse of a mass shell inside which the mass is $M = 4\pi x_i^3 \bar{\rho}_i (1 + \delta_i)/3$, where x_i is the initial radius and δ_i is the initial density contrast within the sphere with the radius x_i (hereafter the subscript i represents the initial time value). The equation of motion (EoM) for the proper radius x of a shell is written as

$$\frac{d^2 x}{dt^2} = -\frac{GM}{x^2}. \quad (3)$$

Equation (3) can be solved analytically, and the solution is given by

$$\begin{aligned} \tilde{t} = \frac{t}{t_i} &= \frac{3}{4\sqrt{1+\delta_i}} \left[1 - \frac{(v_i/H_i x_i)^2}{1+\delta_i} \right]^{-3/2} (\theta - \sin \theta), \\ \tilde{x} = \frac{x}{x_i} &= \frac{1}{2} \left[1 - \frac{(v_i/H_i x_i)^2}{1+\delta_i} \right]^{-1} (1 - \cos \theta), \end{aligned} \quad (4)$$

where t_i is the initial time and v_i is the initial velocity. The solution of Eq. (4) depends only on δ_i and v_i . In order to keep the constant mass $dM/dt = 0$, we give the initial velocity of the shells

$$v_i = H_i x_i \left[1 - \frac{\delta_i}{3(1+\delta_i)} \right], \quad (5)$$

where we assume the matter dominated era, $t \propto a^{3/2}$. The first term represents the Hubble flow and the second term corresponds to the peculiar velocity. According to Eq. (5), the solution, Eq. (4) depends on only the initial density fluctuation, δ_i . Furthermore, we can obtain the critical density contrast that is the density contrast at the collapse time $\theta = 2\pi$ in the linear perturbation theory,

$$\delta_{\text{crit}} = \frac{a(\theta = 2\pi)}{a_i} \delta_i = \frac{3}{5} \left(\frac{3}{2} \pi \right)^{2/3}, \quad (6)$$

where we use the fact that the growth factor of the matter density perturbation is proportional to the scale factor in the matter dominated era.

Next we consider the effect of the homogeneous supersonic relative motion on the nonlinear evolution in the spherical collapse model. A simple extension is to introduce the two kinds of mass shells for dark matter and baryons. Taking into account the supersonic relative motion, the baryon mass shells have the initial bulk velocity, because we take the frame where baryons have the homogeneous relative flow to dark matter. As a result, the collapsing of the baryon mass shells is not spherical and these mass shells are collapsing to the different position from the dark matter shells. However, the collapse of dark matter precedes the one of the baryons in a halo formation and we are interested in a baryon fraction within a collapsed dark matter halo. Therefore, we focus on the dark matter mass shell and, instead of following the evolution of the baryon mass shells, we introduce the baryon mass within the dark matter mass shell, M_b , and rewrite Eq. (3) to

$$\begin{aligned} \frac{d^2 x_c}{dt^2} &= -\frac{G(M_{c,i} + M_b)}{x_c^2}, \\ M_{c,i} &= \frac{4\pi}{3} \bar{\rho}_{c,i} x_{c,i}^3 (1 + \delta_{c,i}), \\ M_b &= \frac{4\pi}{3} \bar{\rho}_b x_c^3 (1 + \delta_b), \end{aligned} \quad (7)$$

where $M_{c,i}$ is the mass within the shell with the initial radius at $x_{c,i}$, x_c is the radius of the mass shell with $M_{c,i}$ at each time, and M_b is the baryon mass in the dark matter shell at the radius x_c . As a shell collapses, the baryon mass M_b inside the shell increases with the growth of δ_b , namely the baryon collapsing. Although the density fluctuation of baryons without the relative motion catches up soon with that of dark matter, the relative motion prevents this process. Therefore, the effect of the relative motion is included through the evolution of M_b . However it is difficult to evaluate analytically M_b with the relative motion. Thus in order to compute Eq. (7), we adopt M_b obtained from the N-body simulation in the following section. We also compare the result based on the spherical collapse model with that from the full N-body simulations in the later section.

III. N-BODY SIMULATION

Besides the analytical way mentioned in the previous section, we evaluate the effect of the supersonic motion between dark matter and baryons on the structure formation at high redshifts by using N-body simulations. In this section, we describe the setup of our N-body simulations.

We perform N-body simulations with the public code Gadget-2 [18]. In all N-body simulations, the cosmological parameters are set to $(\Omega_m, \Omega_b h) = (0.31, 0.69, 0.68)$ with $\Omega_b/\Omega_m \sim 1/6$. The effect of the supersonic relative motion on the structure formation works after the decoupling between photons and baryons. Therefore, the initial redshift for the simulations is $z_i = 1000$. Note that our results almost do not depend on the cosmological parameters because we are interested in the structure formation in the matter dominated era.

For the initial distribution of the particles, we consider the spherical top-hat overdensity region in the isolated system. The simulation box has the uniform distribution of the particles with a uniform overdensity sphere. We set the box size to $L_{\text{Box}} = 200 \text{ kpc}/h$ and the radius of the overdensity sphere to $r_i = 50 \text{ kpc}/h$. Note that we denote hereafter x as the proper distance and r as the comoving distance. In the box, the number of the uniform particles is 3×10^6 and the initial density contrast of dark matter in the over-dense sphere is $\delta_{c,i} = 0.033$. Thus the mass of particles is $2 \times 10^2 M_\odot/h$ and the mass of dark matter within the initial over-density sphere is given by $M_c \sim 4 \times 10^7 M_\odot/h$. Moreover we set the softening parameter to $\epsilon = 0.1 \text{ kpc}/h$. We confirm that changes in these parameters do not affect our result qualitatively.

According to the cosmological perturbation theory, the amplitude of baryon density fluctuations is 1% of that of dark matter density fluctuations with $k = 100 \text{ Mpc}^{-1}$ at $z \sim 1000$. The initial fluctuations of baryons are negligible compared with those of dark matter at $z_i = 1000$. Therefore, we assume that $\Omega_b/\Omega_m (\sim 1/6)$ of the uniform distributed particles is composed of baryons and there is no baryon fluctuation in the overdensity sphere.

Figure 1 shows the initial configuration of the particles. The red dots represent the particle uniformly distributed in the box and the green dots are for the particles included in

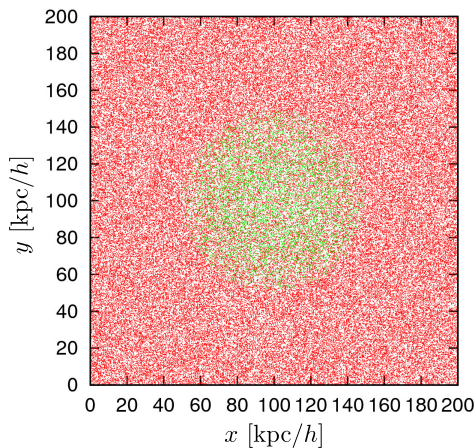


FIG. 1. The initial configuration of the particles. The green particles are contained within the top-hat sphere and the red points are otherwise.

the overdense sphere. Figure 2 shows the initial density contrast of dark matter particles as a function of the radius from the center. In this figure, the red points indicate the values averaged over five realizations of our simulations and the error bars represent the shot noise caused by the finite particle number. The black line is the analytical prediction from our initial condition. This figure tells us that the density is constant in the top-hat sphere. Therefore we can convert the initial position of mass shell to the mass contained within each shell by using the relation $M_{c,i} = 4\pi\bar{\rho}(1 + \delta_i)x_i^3/3$. We set the initial velocity of dark matter given by only the second term of Eq. (5), because N-body simulations are performed in the comoving coordinate.

In order to take into account the supersonic relative motion, we give the additional velocity to all baryons. The correlation of the supersonic relative velocity has the significant value on larger scale than scales of our interest that are smaller than Mpc. Therefore, we assume that all baryons in the simulations have the constant supersonic relative velocity v_{bc} in one direction. In other words, in the simulation, the additional initial velocity for baryons is represented as $\vec{v}_{b,i} = (v_{bc}, 0, 0)$.

All terms related to the relative velocity in Eq. (2) are proportional to kv_{bc} . This fact suggests that the effect of relative motion on the spherical collapse of dark matter halos also depends on a factor $v_{bc}k \propto v_{bc}/M_c^{1/3}$. Thus, instead of changing both the dark matter halo mass M_c and the relative velocity v_{bc} , we perform numerical simulations for different relative velocities (5 km, 15 km, 30 km, 50 km, 100 km, 150 km, 200 km, 300 km, 500 km) with fixing the dark matter halo mass $M_c \sim 4 \times 10^7 M_\odot/h$, in order to evaluate the dependence of the effect of the relative velocity on M_c and v_{bc} .

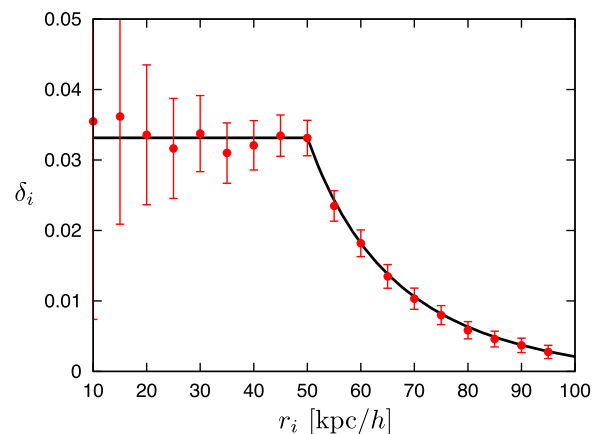


FIG. 2. The initial density contrast distribution of dark matter. The red points are the values averaged five realizations and the error bars show the shot noise caused by the number of particles contained within mass shells. The black line is the analytical prediction.

In the simulations, we use the periodic boundary condition. Therefore, when the relative velocity is higher than 200 km/s, baryon particles leaving the simulation box along the direction of the relative velocity reenter the box from the opposite direction due to the boundary condition. In this case, the distribution of reentering baryons is no longer homogeneous in the perpendicular direction to the relative velocity and, resultantly, the dependence on the boundary condition arises in the results. In order to remove this dependence, we make the perpendicular positions of baryons random when the baryon particles reenter the simulation box.

IV. RESULT

In this section, we present the results of our N-body simulations. First we show the result of the reference model that is the case without the relative velocity. Figure 3 shows the time evolutions of the radii of mass shells from the center. In our simulation, we determined the center of the collapsing shells by using the mean position of the particles contained initially within the top-hat over-density sphere at each time step. In this figure, the red line represents the mass shell containing $0.6M_c$ ($r_i = 42$ kpc/h), and the green and blue lines are for that containing $0.8M_c$ ($r_i = 46$ kpc/h) and M_c ($r_i = 50$ kpc/h), respectively. Additionally the black line corresponds to the analytical solution of the spherical collapse model, Eq. (4), with $\delta_{m,i} = (\bar{\rho}_{c,i}\delta_{c,i} + \bar{\rho}_{b,i}\delta_{b,i})/(\bar{\rho}_{c,i} + \bar{\rho}_{b,i}) = 0.028$ and the velocity v_i given by Eq. (5). Note that the shell evolution of the spherical collapse model depends on $\delta_{m,i}$ only. Therefore, in our initial condition where the overdensity sphere has the homogeneous density profile, the spherical collapse model predicts that all mass shells inside the over-density sphere trace the black dashed line

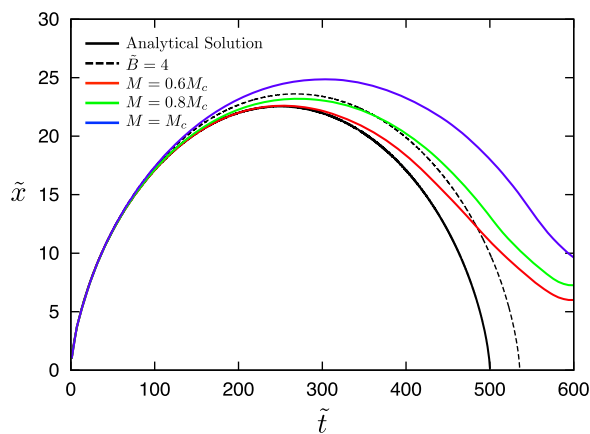


FIG. 3. The evolutions of radii of mass shells containing $0.6M_c$ (red), $0.8M_c$ (green), and M_c (blue). The solid black line is the analytical solution of spherical collapse model with $\delta_{m,i} = 0.028$. The dashed black line is the analytical solution corrected in consideration of the periodic boundary condition with $\tilde{B} = 4$.

and collapse at the same time, independently on the mass contained by the mass shells.

The evolutions of radii of the mass shells from N-body simulations agree with the analytic solution of the spherical collapse model before the turnaround time when the radius reaches the maximum. However, after the turnaround time, the results from N-body simulations deviate from the analytic solution. One of the reasons for this deviation is that the particles cannot be concentrated on the infinitesimal point in N-body simulations. Therefore, the particles in the simulations begin to be relaxed with each other after the turnaround time and the collapse is prevented. Furthermore the shot noise induces the substructures inside the collapsing sphere and the ejection of the particles from the mass shells, and resultantly causes the dispersion of the collapse time as discussed in Ref. [19]. These effects of relaxation and shot noise lead the delay of the collapse and cause the deviation from the analytical solution after the turnaround time.

Figure 3 also shows that the outer mass shells collapse later than the inner ones, although the theoretical spherical collapse model claims that all mass shells collapse at the same time. The reason is the effect of the periodic boundary condition. In order to evaluate this effect simply, we consider the motion of a particle along the x -axis direction with the periodic boundary condition. Since we should take into account the gravitational force from the overdensity region in the other boxes due to the boundary condition, the EoM, Eq. (3), along the x -axis is corrected to

$$\frac{d^2\tilde{x}}{d\tilde{t}^2} = -\frac{2(1+\delta_i)}{9\tilde{x}^2} + \sum_{n=1}^{\infty} \left[\frac{2\delta_i}{9(na\tilde{B}-\tilde{x})^2} - \frac{2\delta_i}{9(na\tilde{B}+\tilde{x})^2} \right], \quad (8)$$

where $\tilde{B} = a_i L_{\text{Box}}/x_i$. When the position of the shell is close to the center of the simulation box at the initial time, \tilde{B} becomes small and vice versa. Namely, the smaller \tilde{B} is, the more efficient the boundary effect is. In our calculation, the most outer shell that contains the mass M_c inside has $\tilde{B} = 4$. The evolution for $\tilde{B} = 4$ is plotted in the black dashed line in Fig. 3.

Figure 4 shows the turnaround time (upper panel) and the reference collapse time (lower panel) in the reference model as functions of the initial radius of the mass shell. Here, the turnaround time and the reference collapse time are defined as the times when the radius of the mass shell becomes maximum and minimum, respectively. In this figure, the red points with the error bars represent the averages and the standard errors obtained from the five realizations of N-body simulations, and the black line corresponds to the theoretical predictions in the spherical collapse model. Moreover the dashed line shows the turnaround time obtained from Eq. (8) which includes the effect of the boundary condition. One can find that the

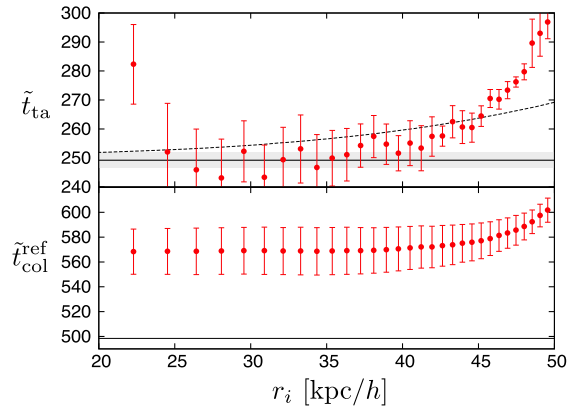


FIG. 4. The turnaround time (upper panel) and the reference collapse time (lower panel). The red points are the results of N-body simulations with the standard error measured five realizations, and the black lines are the analytical predictions. In the upper panel the shaded region shows the error caused from shot noise shown in Fig. 2. The dashed line shows the prediction from the solutions of Eq. (8) with \tilde{B} converted from r_i .

turnaround time is consistent with the theoretical prediction within $r_i = 40$ kpc/h. The one of the reasons why the outer mass shells turn around later is the effect of the periodic boundary condition discussed above. In the case where we take the boundary condition into account, the turnaround time matches the theoretical prediction within $r_i = 43$ kpc/h that corresponds with $M = 0.65M_c$. The difference between the turnaround time estimated from the outer shells than $r_i = 43$ kpc/h and theoretical one is due to the ejections of particles. As we have mentioned, the reference collapse time in N-body simulations delays for all r_i , compared with the theoretical prediction. Additionally, similarly to the turnaround time, the deviation becomes large as r_i increases.

Next we show how the supersonic relative motion affects the collapse in N-body simulations. Performing five realizations for different v_{bc} , we obtain the typical evolution of mass shells by averaging each realization. Figure 5 represents the evolutions of the mass shells containing $0.6M_c$ with four different supersonic relative velocities, $v_{bc} = 30$ km/s (in red), $v_{bc} = 50$ km/s (in green), $v_{bc} = 100$ km/s (in blue), and $v_{bc} = 150$ km/s (in magenta). We can convert the results for different velocities with a fixed mass into those for different masses with a fixed velocity through the dependence of the relative velocity effect on $v_{bc}/M_c^{1/3}$ as mentioned above.

For comparison, the corresponding evolution of the mass shell with $0.6M_c$ in the reference model ($v_{bc} = 0$ km/s) is plotted as the black solid line. As the relative velocity becomes large, the start of the collapse delays and the maximum radius increases. Therefore, we can conclude that the supersonic relative motion prevents the collapse. Additionally we show the solutions of Eq. (7) as the dashed lines in Fig. 5. Solving Eq. (7) numerically, we use the

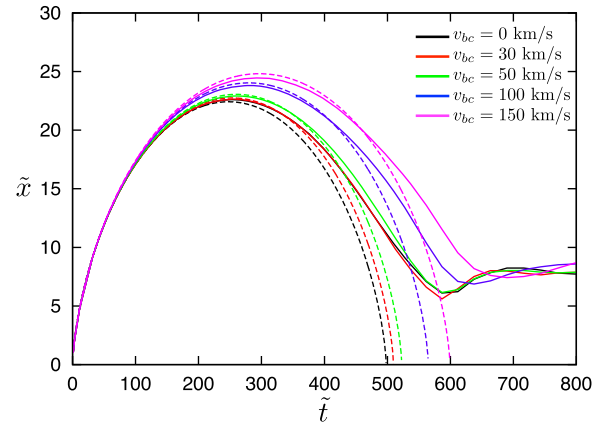


FIG. 5. The evolutions of mass shell containing $0.6M_c$ with supersonic relative velocities $v_{bc} = 30$ km (red), $v_{bc} = 50$ km (green), $v_{bc} = 100$ km (blue), $v_{bc} = 150$ km/s (magenta) and reference model (black). Each dashed line is the solution of Eq. (7) with the baryon density fluctuation derived from N-body simulations.

baryon fluctuation δ_b obtained from the particle data of the N-body simulations within $r_i \leq 42$ kpc/h corresponding to $0.6M_c$. We find that the semianalytical model agrees with the results of N-body simulations before the turnaround time.

To illustrate the delay of the collapse due to the supersonic relative motion we plot the turnaround time and the reference collapse time in Fig. 6 for the different supersonic relative velocities. In this figure, both the turnaround and the reference collapse time are represented as the functions of the initial radius of the mass shell. We show additionally the turnaround times obtained from the solutions of Eq. (7) as the dashed lines in the top panel of Fig. 6. The evaluations of the turnaround time from the semianalytical solutions are consistent with the turnaround times from N-body simulations within $r_i \sim 40$ kpc/h that is same as the reference case. In the following discussions, we use twice the turnaround time as the collapse time. In this case, the scale factor at the collapse time is given by $a_{\text{col}} = (2\tilde{t}_{\text{ta}})^{2/3} a_i$.

V. DISCUSSION

In this section, we show the baryon fraction within the dark matter overdensity sphere. We also discuss the delay of the collapse time and provide the fitting formula of the critical density contrast with the relative motion between dark matter and baryons. Furthermore we present the modification of the halo mass function by taking account of the relative motion.

A. Baryon fraction

First we consider the baryon fraction which represents the mass ratio between baryons and total matter

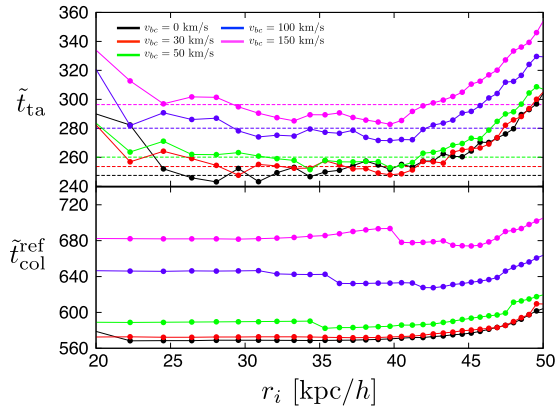


FIG. 6. The turnaround time (upper panel) and the reference collapse time (lower panel) as the function of the initial radius of the mass shell with the supersonic relative velocity $v_{bc} = 30$ km (red), $v_{bc} = 50$ km (green), $v_{bc} = 100$ km (blue), $v_{bc} = 150$ km/s (magenta) and the reference model (black). In the upper panel the dashed lines are the turnaround time estimated from the solution of the semianalytical model.

($f_b = M_b/M_m$) within the dark matter overdensity sphere. The baryon fraction is important not only to estimate the effect of the supersonic relative motion on the collapse of dark matter spheres, but also to discuss the first star formation or observables related with baryons. We calculate the baryon fraction by counting baryon particles within the dark matter collapsing overdensity sphere.

Figure 7 shows the time evolutions of the baryon fraction. As the relative velocity increases, the baryon fraction becomes smaller. In the case with the nonzero relative velocity, the baryon overdensity region is no longer spherically symmetric and the peak position of baryon density is different from that of dark matter, depending on the amplitude of the relative velocity. However, such asymmetry of the baryon distribution does not affect the

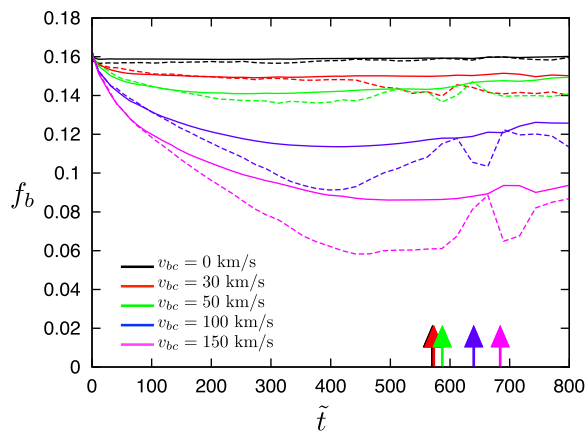


FIG. 7. The baryon fractions within the dark matter overdensity sphere whose initial radius are 50 kpc/h (solid lines) and 42 kpc/h (dashed lines). The arrows show the reference collapse times.

dark matter collapse well. As shown in Fig. 5, the dark matter collapse in the N-body simulations is consistent with the spherical collapse model until the turnaround time. Therefore, we can infer that, in spite of the asymmetric distribution for baryons, the dark matter collapse remains spherical. Around the reference collapse time of the dark matter shells, the baryon fraction estimated within $r_i = 42$ kpc/h starts to oscillate. This is mainly due to the difference of the density peak positions between baryons and dark matter. The baryon overdensity region is attracted by that of dark matter gravitationally and oscillates around. As time goes, the difference of the peak positions will be relaxed and the peak position of baryons is expected to overlap that of dark matter. Note that this result is based on the spherical collapse model which is an ideal isolated system. However, the actual collapse happens with many surrounding effects as shown in cosmological simulations. Therefore, to evaluate the baryon fraction properly, these effects could be not negligible.

B. Delay of the halo formation

The supersonic relative motion delays the collapse time of dark matter halos as shown in Fig. 6. In the spherical collapse model without the relative velocity, the collapse time is dependent on only the initial density fluctuation. However, in the case of the nonzero relative velocity, the collapse time depends on the halo mass M_c and the amplitude of the relative velocity. Additionally, the effect of the relative motion cumulatively becomes large for the small initial density contrast, because the small initial density contrast takes longer time to the collapse. Therefore, the change of the collapse time with the relative velocity is represented as a function of M_c , v_{bc} and $\delta_{c,i}$. We define the correction of the scale factor at the collapse time related with the modification of the critical density contrast, as

$$\mathcal{A}(M_c, v_{bc}, \delta_{c,i}) \equiv \frac{a_{\text{col}}(M_c, v_{bc}, \delta_{c,i}) - a_0(\delta_{c,i})}{a_0(\delta_{c,i})}, \quad (9)$$

where $a_0(\delta_{c,i})$ is the scale factor at the collapse time without the relative velocity between baryons and dark matter.

Figure 8 shows the relative difference \mathcal{A} as a function of the relative velocity with a fixed mass $M_c \sim 4 \times 10^7 M_\odot/h$. We plot \mathcal{A} for different three initial density contrasts estimated from the N-body simulations with our boundary condition (shaded regions) or the usual periodic boundary condition (dashed lines). We find that the effect of the supersonic relative velocity is negligible for velocities smaller than 50 km/s. The relative velocity is small so that baryons are captured gravitationally by the dark matter halo and accrete to the halo. Therefore, we can roughly estimate the threshold velocity as the circular velocity of the dark matter halo at the initial redshift,

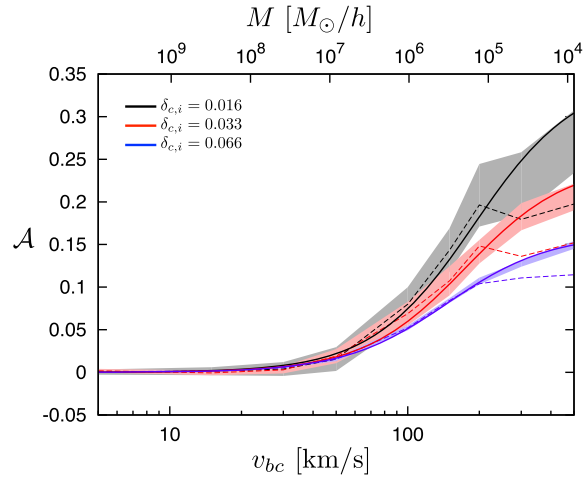


FIG. 8. The relative time difference for the collapse as a function of relative velocity v_{bc} with the halo mass fixed to $M_c \sim 4 \times 10^7 M_\odot/h$ and three initial density fluctuations $\delta_{c,i} = 0.016$ (black), $\delta_{c,i} = 0.033$ (red), and $\delta_{c,i} = 0.066$ (blue) evaluated from turnaround time. The shaded regions show the standard error region from the N-body simulation. The solid lines are the fitting formula Eq. (12). The dashed lines are results from the N-body simulations with the usual periodic boundary condition. The upper horizontal axis shows the mass converted with $v_{bc} = 30$ km/s.

$$v_{\text{cir}} = \sqrt{\frac{GM_c}{x_i}} \approx 57 \left(\frac{M_c}{3.85 \times 10^7 M_\odot} \right)^{1/3} \text{ km/s}. \quad (10)$$

This criterion can be also obtained from the condition that the third term related to the relative velocity, $\mu^2 k^2$, dominates in the right-hand side in the second equation of Eq. (2). Therefore, when the relative velocity is larger than the criterion velocity, the relative motion prevents the collapse by the third term in Eq. (2). Similarly, when the relative velocity is larger than v_{cir} , the effect of the relative motion on the structure formation arises. The upper horizontal axis represents the corresponding mass in the case of a fixed velocity $v_{bc} = 30$ km/s, which is converted through the $v_{bc}/M_c^{1/3}$ -dependence of the relative motion effect. Thus one can find that the supersonic relative motion does not affect the formation of dark matter halos with mass larger than $M_c \gtrsim 10^7 M_\odot/h$ for $v_{bc} = 30$ km/s which corresponds to the effective Jeans scale discussed in Sec. II A.

In the N-body simulation results with the usual periodic boundary condition, the modification becomes independent of the amplitude of the relative velocity in the case with $v_{bc} \gtrsim 200$ km/s shown in Fig. 8. However this independence is due to the artificial condition of the simulations. When $v_{bc} \gtrsim 200$ km/s, all baryons can travel a distance larger than the simulation box size L_{Box} until $\tilde{t} \sim 100$ and are attracted gravitationally twice by the collapsing dark matter sphere. Therefore, the effect of the relative velocity

seems to be saturated in this relative velocity region. On the other hand, the results of the N-body simulations with our boundary condition shown as the shaded region in Fig. 8 are not saturated. In order to verify the validity of the result of our N-body simulations, we show the collapse time and the baryon fraction in the limit of the large homogeneous relative velocity. One can easily imagine that, when the relative velocity is enough high ($v_{bc} = 500$ km/s), which corresponds to very small dark matter halos ($M_c \sim 10^4 M_\odot/h$) in the case of $v_{bc} = 30$ km/s, baryons do not collapse along the relative velocity direction. In this limit, we can ignore the gravitational force from the dark matter halo on the baryon motion along the relative velocity direction. In other words, the gravitational collapsing of baryons occurs perpendicular to the relative velocity direction and does not along the parallel direction. Therefore, to evaluate the evolution of the density fluctuations, it is useful to consider the motion of baryons with the relative velocity in the comoving cylindrical coordinate system whose axis is parallel to the relative velocity motion. In this case, the EoM of baryons particles with the initial velocity $(v_{b\parallel}, v_{b\perp}) = (v_{bc}, 0)$ is given as

$$\begin{aligned} \frac{d^2 \vec{r}_b}{dt^2} &= -2H\vec{v}_b - \frac{G\delta M_c}{a^3 r_b^3} \vec{r}_b, \\ \delta M_c &= \frac{4}{3} \pi \bar{\rho}_c [r_{c,i}^3 (1 + \delta_{c,i}) - r_c^3] \\ &\quad \times \max[1, (r_b/r_c)^3], \end{aligned} \quad (11)$$

where r_b is the radial component of \vec{r}_b from the center of the dark matter sphere and r_c is the radius of the overdensity sphere of dark matter. Note that we ignore the gravitational force of the baryon fluctuation in Eq. (11), because $\delta M_b \ll \delta M_c$. We solve Eqs. (7) and (11) numerically with different initial positions $\vec{r}_{b,i}$ chosen randomly. We calculate the resultant baryon density contrast in a collapsing spherical shell of dark matter by taking the average of $\delta_b = (r_{b\perp}/r_{b\parallel})^2 - 1$ for baryons inside the shell of dark matter, because the collapse of baryons is cylindrical.

Figure 9 shows the evolution of the baryon fractions with $M_c \sim 4 \times 10^7 M_\odot/h$ and $v_{bc} = 500$ km/s. The red solid line represents the solution obtained with the periodic boundary condition. In order to take into account the periodic boundary condition, we solve Eqs. (7) and (11) with the assumption that the position of baryons, \vec{r}_b , is limited within the box size and baryons return into the box from the opposite side when they exit from one side of the box. For comparison, we also solve the equations without the boundary condition and plot the solution in the blue solid line. Baryons with the periodic boundary condition feel gravitational force stronger than without the boundary condition. Therefore, the collapse is faster with the boundary condition than without the boundary condition.

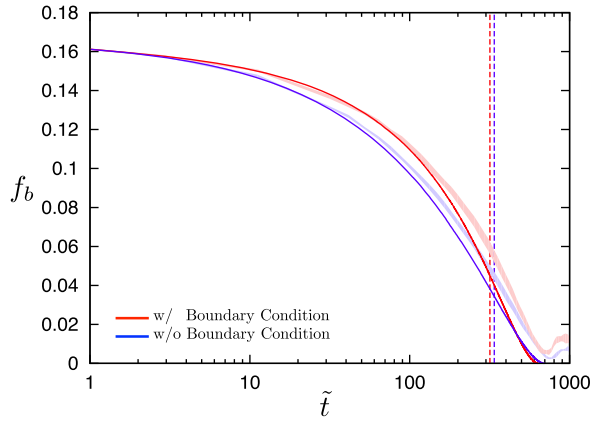


FIG. 9. The baryon fractions within the dark matter halo ($r_i = 42 \text{ kpc}/h$) with $M_c \sim 4 \times 10^7 M_\odot/h$ and $v_{bc} = 500 \text{ km/s}$ and solution of Eqs. (7) and (11) with or without the periodic boundary condition (red or blue line). The each color shaded region show the 1σ dispersion of the baryon fractions estimated from five realizations of N-body simulations. The vertical dashed lines show the turnaround times from N-body simulations.

Moreover, in Fig. 9, we show the results from N-body simulations. The red shaded region represents the standard error region from the N-body simulations with the periodic boundary condition, while the blue shaded region gives the standard error region for the N-body simulations with our boundary condition which is the periodic boundary condition with the position shuffling of the baryon particles reentering into the box. In Fig. 9, N-body simulations with our boundary condition is consistent with the numerical solution without the periodic boundary condition, while N-body simulations with the periodic boundary condition agrees with the solution with the periodic boundary condition. We find that, in the both boundary condition cases, the differences between the numerical solutions and N-body simulations arise around $\tilde{t} \approx 100$. This is because, as the collapse proceeds, the baryon density in the N-body simulations grows as the spherical collapse rather than the cylindrical one. Therefore, the baryon fraction is larger in N-body simulations than in the numerical calculations.

In addition, we plot \mathcal{A} as functions of the initial density fluctuations $\delta_{c,i}$ with $M_c \sim 4 \times 10^7 M_\odot/h$ and $v_{bc} = 500 \text{ km/s}$ in Fig. 10. The red and blue solid lines are obtained from the numerical calculations with and without the periodic boundary condition, respectively. In the case with the periodic boundary condition, we overestimate the gravitational force to collapse as mentioned above and, therefore, the delay of the collapse is not larger than in the case without the boundary condition. For comparison, we plot the black solid line which represents the results with the assumption that baryons cannot collapse. The difference from the black solid line represents the contribution due the collapse of the baryon component. When the relative velocity is large enough, baryons cannot collapse to the dark matter mass shell. Accordingly, as the relative

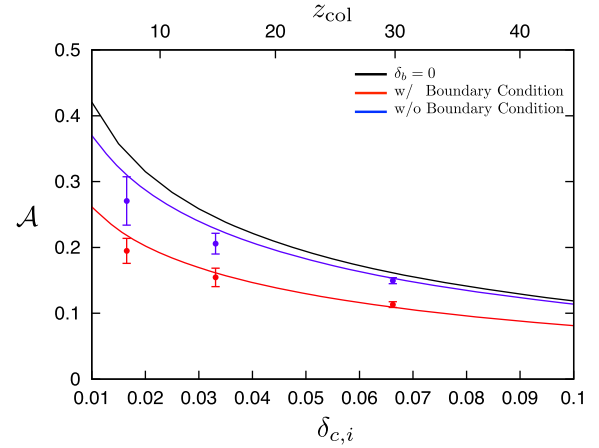


FIG. 10. The collapse time with $M_c \sim 4 \times 10^7 M_\odot/h$ and $v_{bc} = 500 \text{ km/s}$ estimated by solving Eqs. (7) and (11) with boundary condition (red) and without boundary condition (blue). The black solid line is corresponded the solution of Eqs. (7) with $\delta_b = 0$ at any time. Points represent estimations from N-body simulations with $v_{bc} = 500 \text{ km/s}$. The upper axis presents the collapse time from Eq. (4) with the total matter density fluctuation $\delta_{m,i} = \bar{\rho}_c \delta_{c,i} / (\bar{\rho}_c + \bar{\rho}_b)$.

velocity becomes large, the blue solid line shifts to the black line. We also plot the results of N-body simulations with the periodic boundary condition and our boundary condition as red and blue points with the standard error bars in Fig. 10, respectively. As shown in Fig. 9, the numerical calculation with the periodic boundary condition agrees with N-body simulations with the periodic boundary condition, while the numerical calculation without the boundary condition is consistent with N-body simulations with our boundary condition. We remind you that our boundary condition is introduced to remove the artificial distribution of the reentering baryon particles due to the periodic boundary condition in N-body simulations. We conclude that the saturation in \mathcal{A} from N-body simulations with the periodic boundary condition is caused by this artifact. The results from N-body simulations with our boundary condition present realistic phenomena.

Based on the results of our N-body simulations, we find the fitting formula of \mathcal{A} represented as the solid lines in Fig. 8. The fitting formula is given by

$$\mathcal{A}(M_c, v_{bc}, \delta_{c,i}) = \mathcal{A}_{\delta_b=0}(\delta_{c,i}) \frac{\mathcal{B}^\nu(M_c, v_{bc}, \delta_{c,i})}{\mathcal{B}^\nu(M_c, v_{bc}, \delta_{c,i}) + 1},$$

$$\mathcal{B}(M_c, v_{bc}, \delta_{c,i}) = \frac{v_{bc}}{v_{\text{norm}}(\delta_{c,i})} \left(\frac{M_c}{3.85 \times 10^7 M_\odot/h} \right)^{-1/3},$$

$$v_{\text{norm}}(\delta_{c,i}) = a_v - b_v \delta_{c,i}, \quad (12)$$

where $\mathcal{A}_{\delta_b=0}$ is the solution of Eq. (7) with $\delta_b = 0$ shown in Fig. 10, and ν , a_v and $b_v > 0$ are the fitting parameters. The velocity v_{norm} is the critical velocity for the collapse of baryons along the direction of the relative velocity. When

$v_{bc} \gg v_{\text{norm}}$, the relative velocity is much larger than v_{circ} even at the collapse time and baryons does not collapse along the direction of the relative velocity as mentioned above. Since the collapse time becomes long with decreasing δ_i and v_{bc} is inversely proportional to the scale factor, v_{norm} increases as δ_i decreases. Thus we conclude that the delay is controlled by two critical velocity v_{circ} and v_{norm} . Nevertheless it can be calculated numerically, we use the approximated function of $\mathcal{A}_{\delta_b=0}$,

$$\mathcal{A}_{\delta_b=0}(\delta_{c,i}) = \frac{\delta_{c,i}^{-0.146} - 1.06}{4.12 \times \delta_{c,i}^{0.648} + 1.93}. \quad (13)$$

We estimate the parameters by fitting simultaneously Eq. (12) to \mathcal{A} with using three different initial density fluctuations. Furthermore we perform a Fisher analysis and obtain the parameters as

$$\nu = 2.02 \pm 0.07, \quad a_v = 205 \pm 16, \quad b_v = 877 \pm 253, \quad (14)$$

where the standard errors are estimated after marginalizing over other parameters. Since we sample the data for three different initial conditions, the parameter b_v has a large error. However, we find that the form in Eq. (12) fits well with the N-body simulation results.

C. Mass function

The delay of the halo formation due to the relative velocity modifies the abundance of dark matter halos. In this section, we evaluate the modification based on the Press-Schechter formalism. In the Press-Schechter formalism, the delay of the collapse is represented as the increase of the critical density contrast. Using the relative time difference \mathcal{A} , we can write the modified critical density contrast during the matter dominated era as

$$\tilde{\delta}_{\text{crit}}(M_c, v_{bc}, \delta_{c,i}) = \delta_{\text{crit}}[1 + \mathcal{A}(M_c, v_{bc}, \delta_{c,i})]. \quad (15)$$

The critical density contrast depends on the relative velocity in the region where the collapses happens. Therefore, the modified halo mass distribution can be written with the probability distribution function of the amplitude of the relative velocity at the initial time $f(v_{bc})$ as

$$\begin{aligned} \tilde{n}(M_c, z) &= \int dv_{bc} f(v_{bc}) \sqrt{\frac{2}{\pi}} \frac{\tilde{\rho}(z) \tilde{\delta}_{\text{crit}}(M_c, v_{bc}, \delta_{c,i})}{M_c \sigma(M_c, z)} \\ &\times \left[\frac{d \ln \tilde{\delta}_{\text{crit}}(M_c, v_{bc}, \delta_{c,i})}{dM_c} - \frac{d \ln \sigma(M_c, z)}{dM_c} \right] \\ &\times \exp \left[-\frac{\tilde{\delta}_{\text{crit}}^2(M_c, v_{bc}, \delta_{c,i})}{2\sigma^2(M_c, z)} \right]. \end{aligned} \quad (16)$$

Note that, because of the existence of the relative motion, the redshift of the collapse time depends not only on the initial density fluctuation of cold dark matter, but also on the halo mass M_c and the amplitude of relative velocity v_{bc} . Therefore, in Eq. (16), the mass derivative term of the critical density additionally arises because the mass dependence of the critical density contrast affects the hierarchical structure formation.

We assume that the probability distribution $f(v_{bc})$ follows the Maxwell-Boltzmann distribution because the each component of relative velocity is independent and obey the same Gaussian distribution whose mean value is zero and the dispersion is σ_v ;

$$f(v_{bc}) dv_{bc} = 4\pi v_{bc}^2 \left(\frac{3}{2\pi\sigma_v^2} \right)^{3/2} \exp \left(-\frac{3v_{bc}^2}{2\sigma_v^2} \right) dv_{bc}, \quad (17)$$

where we use $\sigma_v = 28.8$ km/s according to the latest cosmological parameters from PLANCK paper [20] and we use CAMB [21] to calculate $\sigma(M_c, z)$.

Figure 11 shows the ratio between the mass function with and without the relative velocity. Here we plot the ratio at four different redshifts, $z = 10, 15, 20,$ and 30 . These lines are evaluated by using the fitting formula Eqs. (12) for \mathcal{A} in Eq. (15). The suppression of the mass function due to the relative motion is more significant for smaller masses region and at higher redshifts. At $z = 30$, although the modification \mathcal{A} is very small around $10^7 M_\odot/h \lesssim M_c \lesssim 10^9 M_\odot/h$, the suppression of the mass function is not negligible. This is because such massive halos at high redshifts are rare objects which satisfy $\tilde{\delta}_{\text{crit}} \gg \sigma(M_c)$ in the Press-Schechter formalism. Therefore, the effect of the modification \mathcal{A} appears exponentially in the Press-Schechter formalism, even if \mathcal{A} is small. The ratio of the mass functions reaches the minimum at $M_c \sim 10^5 M_\odot/h$. On smaller scales than $M_c \sim 10^5 M_\odot/h$, the suppression of the mass function decreases because the

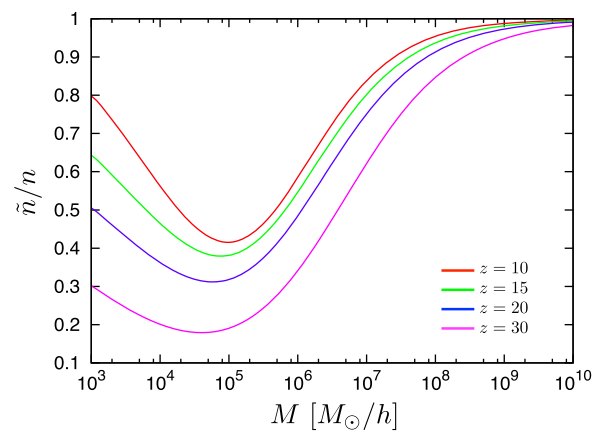


FIG. 11. The ratio of mass function of the dark matter halo between with and without relative motion at four redshifts $z = 10$ (red), $z = 15$ (green), $z = 20$ (blue), and $z = 30$ (magenta).

mass derivative term of the critical density in Eq. (16) increases around $M_c \sim 10^5 M_\odot/h$ as shown in Fig. 8.

Figure 11 also shows that the mass function is suppressed even around the EoR ($z \sim 10$). This is because the redshift dependence of the derivative terms in Eq. (16) is weak. Although the suppression scales are consistent, the suppression of mass function around EoR is stronger than in other previous works. Especially Ref. [12] reported that the suppression disappears at $z \sim 10$ in their SPH simulations. Of course, unlike the SPH simulations, we only simulate the gravitational force, ignoring the baryon physics. However, it is worth mentioning reasons of the difference between our calculation of the mass function and previous work in term of the gravitational growth. The first reason for this difference is that we do not include the environmental effects of the structure formation, e.g., an accretion of other density peaks of baryons neighboring the dark matter halo. These effects increase the baryon fraction within a dark matter halo and promotes the halo formation. The second reason is that the relative motion produces halos derived from offsetting baryon peaks [22]. This effect increases simply the number of halos. It is difficult to include this effect in the Press-Schechter formalism. We will be able to estimate a number of halos originated from the baryon peaks by applying the our simulations or our semianalytical model of Eq. (7). Finally, the initial condition for matter density and velocity fields is still debatable in the numerical simulations with the relative velocity. In our simulation, we use the initial condition that leads to the maximum delay of the collapse time. Thus the halo mass function in Fig. 11 is calculated on the basis of the optimistic case where the baryons can escape most efficient from the dark matter halo.

VI. SUMMARY

The relative motion between baryons and dark matter plays an important role, particularly, in small-scale structure formation at high redshifts. We have studied their effect on the dark matter halo formation.

We have evaluated the delay of the dark matter halo collapse due to the supersonic relative motion by using the cosmological N-body simulation. We have found that the delay of the collapse becomes large for a dark matter halo with $M_c \sim 4 \times 10^7 M_\odot/h$, when the relative velocity is larger than $v_{\text{cir}} = 57$ km/s. In other words, the delay of the collapse happens when the relative velocity is larger than the typical circular velocity of the dark matter halo. Moreover, we have shown that the supersonic relative motion delays the fall of baryons into the potential well of the dark matter halo in the context of the spherical collapse model. We have also evaluated the baryon fraction M_b/M_m

of the dark matter halos with the supersonic relative motion by the N-body simulation. The baryon fraction becomes smaller as the amplitude of the relative motion increases. We have pointed out that, when the relative velocity is large enough to escape from the potential of dark matter halos, baryons can collapse only along the perpendicular direction of the relative velocity, like the cylindrical collapse. Furthermore we show the delay of the collapse time for dark matter halo by the relative motion depends on the initial density fluctuation within dark matter spheres, which determines the collapse time of the dark matter halo without relative motion. The smaller initial density fluctuation leads to longer time during which the supersonic relative motions affect the halo collapse. In consequence, the effect of the relative motion is more efficient on dark matter halos formed at later time.

Finally we have estimated the suppression of the abundance of dark matter halos by supersonic relative motion in the context of the spherical collapse model. In the Press-Schechter formalism, the delay of the collapse increases the critical density contrast for the collapse. We have found the fitting formula of the critical density contrast depending on the halo mass, the initial density fluctuations, and the relative velocity. Using the fitting formula, we have calculated the mass function of dark matter halos. The relative motion decreases the mass function with mass smaller than $10^8 M_\odot/h$ before EoR. In particular, the abundance of halos with $M_c = 10^5 M_\odot/h$ is suppressed by 80% at $z = 30$ and a half at $z = 10$.

The delay of the dark matter halo collapse and the decrease of the baryon fraction in dark matter halos due to the relative motion can give the effect on first star formation and the reionization history [23–25]. Such effect could impact the cosmological signals of the EoR including the CMB polarization [26], the redshifted 21 cm lines [27,28] and these cross-correlation [29]. Moreover, the relative motion between dark matter and baryons influences the large scale structure, e.g., baryon acoustic oscillation [30–32], and there is the challenging work detecting this effect by using the results of galaxy distribution from two independent galaxy spectroscopic survey [33]. Based on the results of this paper, we will investigate the effect of the relative motion on the cosmological signals probed by ongoing or planned observations.

ACKNOWLEDGMENTS

This work was supported by JSPS KAKENHI Grants No. 26-2667 (S. A.), No. 24340048 (K. I.) and No. 15K17646 (H. T.). H. T. also acknowledges the support by MEXT’s Program for Leading Graduate Schools PhD professional, “Gateway to Success in Frontier Asia”.

- [1] É. Aubourg, S. Bailey, J.E. Bautista, F. Beutler, V. Bhardwaj, D. Bizyaev, M. Blanton, M. Blomqvist, A. S. Bolton, J. Bovy *et al.*, *Phys. Rev. D* **92**, 123516 (2015).
- [2] R. Adam, P. A. R. Ade, N. Aghanim, Y. Akrami, M. I. R. Alves, M. Arnaud, F. Arroja, J. Aumont, C. Baccigalupi *et al.* (Planck Collaboration), [arXiv:1502.01582](https://arxiv.org/abs/1502.01582).
- [3] S. R. Furlanetto, S. P. Oh, and F. H. Briggs, *Phys. Rep.* **433**, 181 (2006).
- [4] J. R. Pritchard and A. Loeb, *Rep. Prog. Phys.* **75**, 086901 (2012).
- [5] Y. Oyama, A. Shimizu, and K. Kohri, *Phys. Lett. B* **718**, 1186 (2013).
- [6] K. Kohri, Y. Oyama, T. Sekiguchi, and T. Takahashi, *J. Cosmol. Astropart. Phys.* **09** (2014) 014.
- [7] H. Shimabukuro, K. Ichiki, S. Inoue, and S. Yokoyama, *Phys. Rev. D* **90**, 083003 (2014).
- [8] <http://www.mwatelescope.org>.
- [9] <http://www.skatelescope.org>.
- [10] D. Tselikhovich and C. Hirata, *Phys. Rev. D* **82**, 083520 (2010).
- [11] A. Stacy, V. Bromm, and A. Loeb, *Astrophys. J. Lett.* **730**, L1 (2011).
- [12] S. Naoz, N. Yoshida, and N. Y. Gnedin, *Astrophys. J.* **747**, 128 (2012).
- [13] S. Naoz, N. Yoshida, and N. Y. Gnedin, *Astrophys. J.* **763**, 27 (2013).
- [14] A. Fialkov, *Int. J. Mod. Phys. D* **23**, 1430017 (2014).
- [15] S. Naoz and R. Barkana, *Mon. Not. R. Astron. Soc.* **362**, 1047 (2005).
- [16] D. Tselikhovich, R. Barkana, and C. M. Hirata, *Mon. Not. R. Astron. Soc.* **418**, 906 (2011).
- [17] S. Naoz, N. Yoshida, and R. Barkana, *Mon. Not. R. Astron. Soc.* **416**, 232 (2011).
- [18] V. Springel, *Mon. Not. R. Astron. Soc.* **364**, 1105 (2005).
- [19] T. Worrakitpoonpon, *Mon. Not. R. Astron. Soc.* **446**, 1335 (2015).
- [20] P. A. R. Ade, N. Aghanim, C. Armitage-Caplan, M. Arnaud, M. Ashdown, F. Atrio-Barandela, J. Aumont, C. Baccigalupi, A. J. Banday *et al.* (Planck Collaboration), *Astron. Astrophys.* **571**, A16 (2014).
- [21] A. Lewis, A. Challinor, and A. Lasenby, *Astrophys. J.* **538**, 473 (2000).
- [22] S. Naoz and R. Narayan, *Astrophys. J. Lett.* **791**, L8 (2014).
- [23] T. H. Greif, S. D. M. White, R. S. Klessen, and V. Springel, *Astrophys. J.* **736**, 147 (2011).
- [24] U. Maio, L. V. E. Koopmans, and B. Ciardi, *Mon. Not. R. Astron. Soc.* **412**, L40 (2011).
- [25] A. Fialkov, R. Barkana, D. Tselikhovich, and C. M. Hirata, *Mon. Not. R. Astron. Soc.* **424**, 1335 (2012).
- [26] S. Ferraro, K. M. Smith, and C. Dvorkin, *Phys. Rev. D* **85**, 043523 (2012).
- [27] J. M. Bittner and A. Loeb, [arXiv:1110.4659](https://arxiv.org/abs/1110.4659).
- [28] M. McQuinn and R. M. O'Leary, *Astrophys. J.* **760**, 3 (2012).
- [29] H. Tashiro, N. Aghanim, M. Langer, M. Douspis, and S. Zaroubi, *Mon. Not. R. Astron. Soc.* **389**, 469 (2008).
- [30] J. Yoo, N. Dalal, and U. Seljak, *J. Cosmol. Astropart. Phys.* **07** (2011) 018.
- [31] Z. Slepian and D. J. Eisenstein, *Mon. Not. R. Astron. Soc.* **448**, 9 (2015).
- [32] J. Yoo and U. Seljak, *Phys. Rev. D* **88**, 103520 (2013).
- [33] F. Beutler, C. Blake, J. Koda, F. Marin, H.-J. Seo, A. J. Cuesta, and D. P. Schneider, [arXiv:1506.03900](https://arxiv.org/abs/1506.03900).